10

Scanning Image-sensor System for Measurement of Micro-dimensions

10.1 Introduction

Measurement of micro-dimensions such as length, depth, width and radius of the nanomanufactured micro-structures is an important task for precision nanometrology. Some of the micro-structures are made on the workpiece over a long stroke and the measurement of the micro-dimension must be made over the entire stroke. In such cases, it requires the measurement system to have fast enough measuring speed.

An image-sensor system, which consists of an objective lens and an image sensor, is a good candidate for measurement of micro-dimensions [1–5]. Image sensors, including area-image sensors and line-image sensors, have the advantages of non-contact, high speed, as well as high resolution when an objective lens with a high magnification is employed. Image-sensor systems always have the disadvantage of a small field of view when they are used for the measurement of micro-dimensions over a long stroke. This can be overcome by scanning the system over the micro-dimension. However, there are a number of challenges for the scanning image sensor systems. One is the influence of scanning motion errors. Because the depth of focus of a high-magnification objective lens is small, typically on the order of several micrometers, scanning error motions larger than the depth of focus will introduce measurement errors. This is especially a challenge for a micro-dimension measurement over a long stroke. Another challenge is how to provide three-dimensional information of the micro-dimension in a short measurement time because the image provided by the image-sensor system is only a two-dimensional projection of the three-dimensional structure. To make a three-dimensional measurement possible, it is necessary to move the image-sensor system along the optical axis to take multiple images, which makes the measurement of the micro-dimension over a long stroke time-consuming.

In this chapter, two scanning image-sensor systems are presented for fast and accurate measurement of the micro-width of a long slit and the micro-radius of a long edge, respectively.

10.2 Micro-width Measurement by Scanning Area-image Sensor

10.2.1 Micro-width of Long Tool Slit

Measurement of the micro-width of a tool for slot die coating is discussed in Section 10.2. The slot die coating is for applying liquid coatings, such as adhesives and low-viscosity liquids [6]. A slot die is employed as the coating tool in this technology [7]. The main function of the coating tool is to spread liquids into the substrate film as shown in Figure 10.1. The tool has a slit length of several meters and a width on the order of 100 μm, from which the applied liquids come out (Figure 10.2). The slit is formed by two pieces of precision elements, which are machined by a precision grinding machine. Each of the precision parts has a flat area with a dimension of up to several meters in the *X*-direction and several hundred millimeters in the *Y*-direction. The deviations of the slit width, which greatly influence the performance of the coating tool, are required to be less than several micrometers over the entire slit. Measurement of the slit width deviation is thus essential for the process control in the manufacturing of the coating tool [8].

Conventionally, the slit width is measured by using a mechanical thickness gauge point by point along the *X*-direction of the slit as shown in Figure 10.2. The measurement, which relies on the skill of the operator, is time-consuming and lacks accuracy. There also exits a possibility of damaging the edge of the slit. Although it is possible to carry out the slit width measurement by scanning a displacement

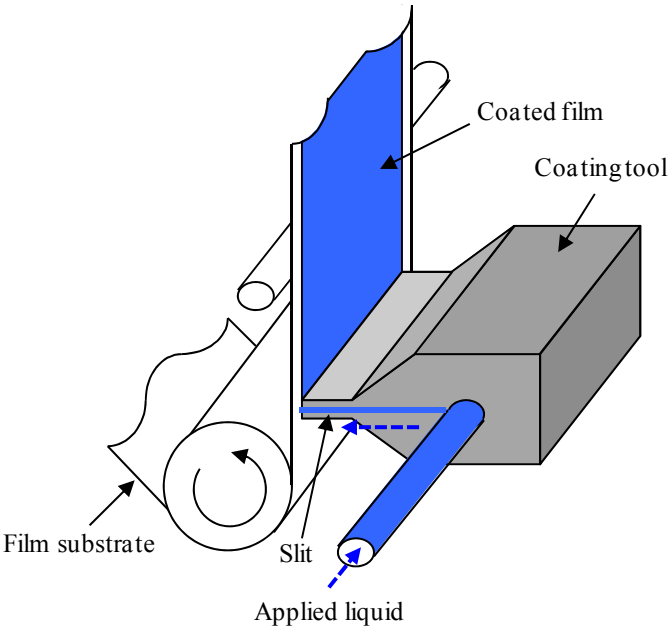

Figure 10.1. A schematic of the slot die coating

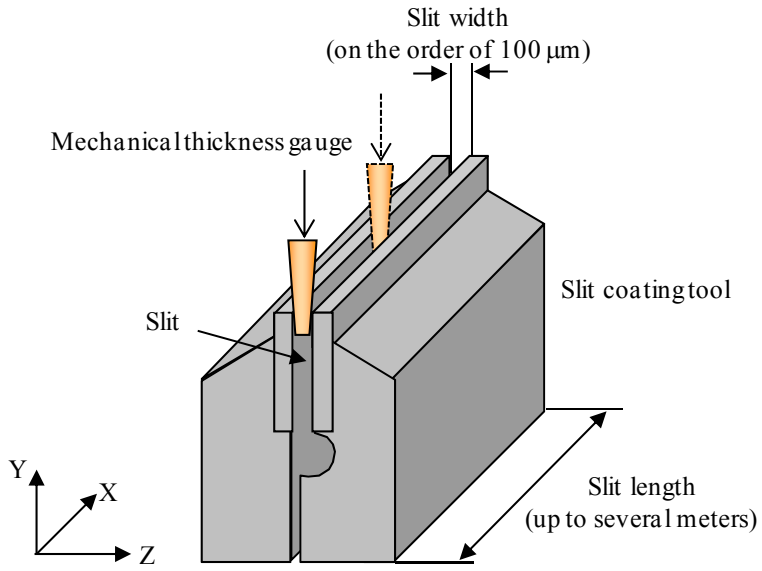

Figure 10.2. The coating tool with a long slit and the conventional measurement method using a mechanical thickness gauge

sensor across the slit along the *Z*-direction, the measurement accuracy is influenced by the edge affect of the sensor and the error motion of the scanning mechanism. The measurement time is also too long.

In Section 10.2, a scanning area-image-sensor method is presented for micro-slit measurement of the coating tool. This method, in which the slit width on the top surface of the slit is scanned by an area-image sensor along the *X*-direction, can be expected to provide non-contact, fast and accurate measurements.

10.2.2 Evaluation of Slit Width

Figure 10.3 shows a schematic of the slit width measurement by using an area-image sensor [9]. An area-image sensor with an objective lens is mounted on the top of the slit to take the image of the slit. The numbers of pixels of the area-image sensor are 720 and 480 in the *Z*-direction and the *X*-direction, respectively. The magnification of the objective lens is set to be 450. The field of view of the image is 680 μm (*Z*) × 510 μm (*X*). Figure 10.4 shows a part of the original image of the slit area taken by the image sensor. The dark area of the image is the slit part since no lights were reflected back to the image sensor. The white area is the top surface of the precision element forming the slit.

Figure 10.5 shows a close-up view of the edge part (part A) in Figure 10.4. It can be seen that the boundary in the image between the areas of the slit and the top surface of the precision element is not clear because of the defocus caused by the slope of the top surface of the precision element. To identify the boundary of the slit, the binary image [10] shown in Figure 10.6 is evaluated by making the image processing as follows:

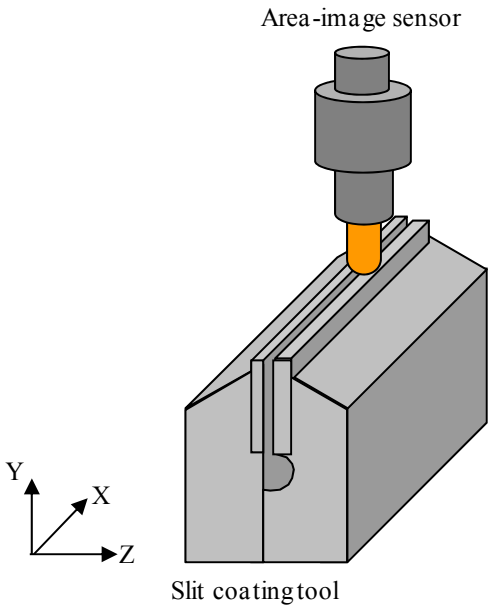

Figure 10.3. The slit width measurement method by using an array image sensor

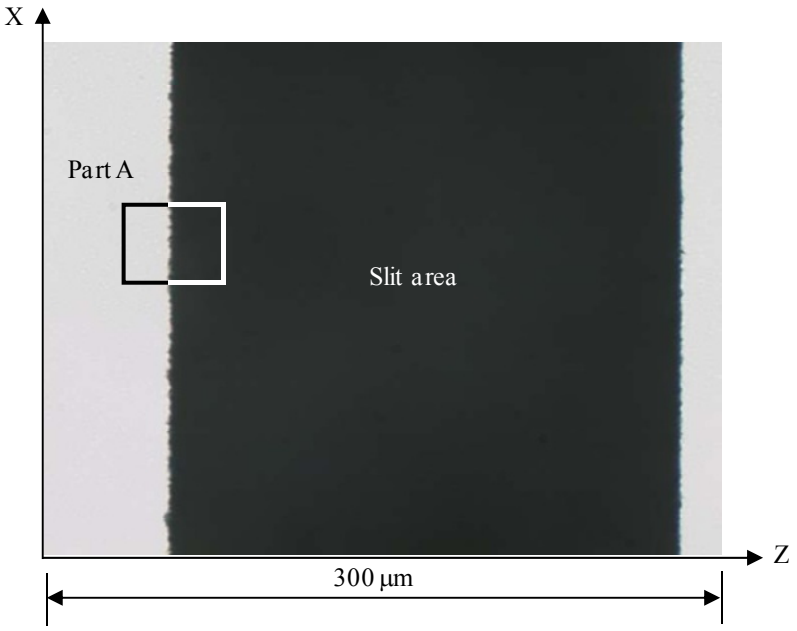

Figure 10.4. Original static image of the slit area by the array image sensor

$$I_B(x,z)=\begin{cases}255 & \left(I(x,z)\geq T\right)\\ 0 & \left(I(x,z)<T\right)\end{cases}, \tag{10.1}$$

where $I(x, z)$ is the original intensity of the pixel of the area-image sensor at the coordinate of (x, z). $I(x, z)$ ranges from 0 to 255. $I_B(x, z)$ is the intensity of the binary image, which is either 0 or 255. T is the threshold value. Figure 10.7 shows the binary image of Figure 10.4. Figure 10.8 shows the intensities of the line BB' in Figure 10.7 before and after the binary processing. As seen in the figures, the boundary of the edge becomes clear after the binary processing.

Figure 10.7 also shows the range for evaluation of the slit width at a position x_i along the X-direction. To reduce the influence of the random errors, the binary data of N line pixels along the X-direction are employed. The slit width is evaluated by averaging the data over this range.

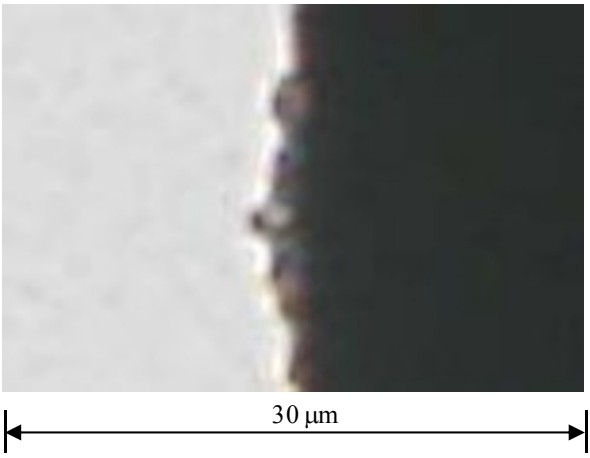

Figure 10.5. Close-up view of the edge area (part A)

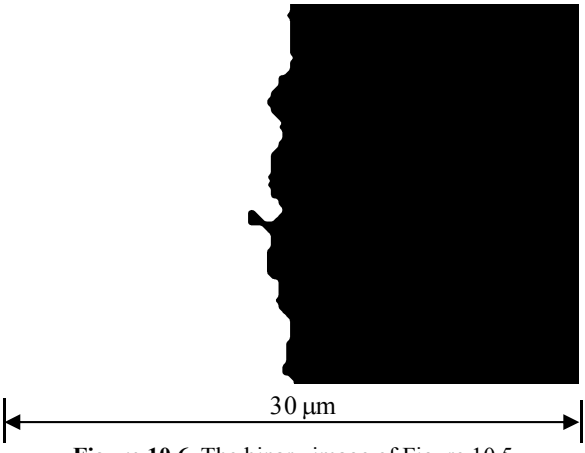

Figure 10.6. The binary image of Figure 10.5

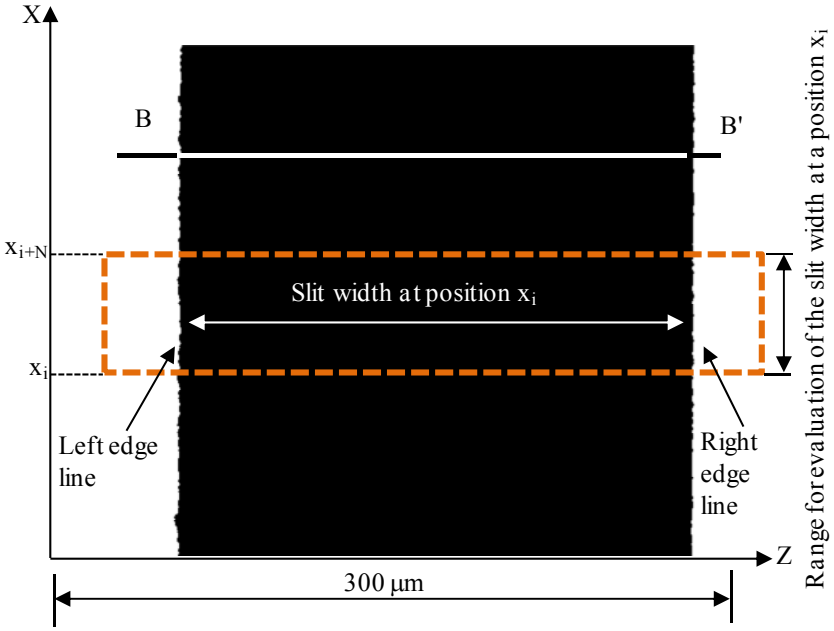

Figure 10.7. The binary image of Figure 10.4

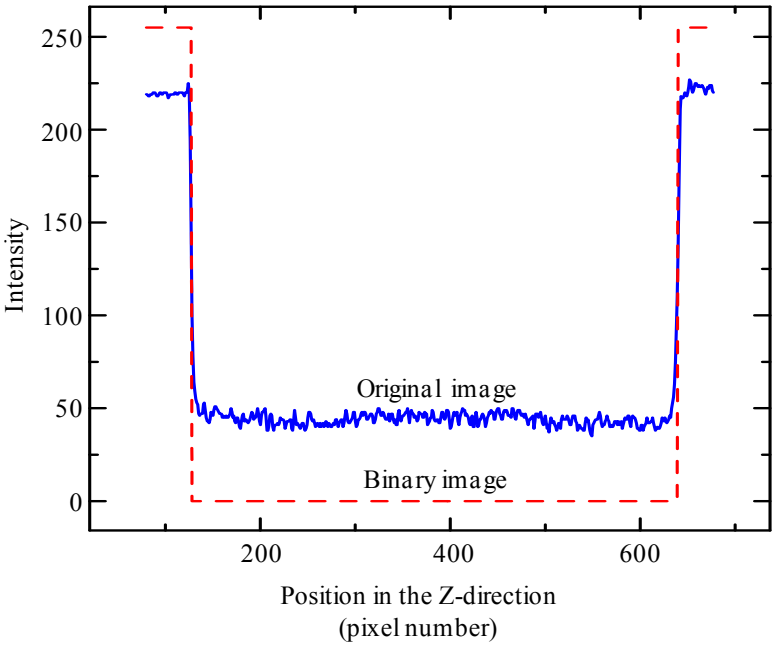

Figure 10.8. Intensity distribution of the cross-section *BB*' in Figure 10.7

10.2.3 Scanning Area-image Sensor

The slit width over the entire slit can be measured by scanning the area-image sensor with a moving stage as shown in Figure 10.9. There are two scanning modes for the measurement. In mode 1, the area-image sensor moves step by step along the *X*-direction. At each step, the area-image sensor takes a static image of the slit. This type of measurement is simple but time-consuming. In mode 2, the image sensor is moved along the *X*-direction at a constant speed to take a video of the slit. The measurement time can be greatly shortened in this scanning mode. Assume that the time to take one frame of image is *T* seconds and the scanning velocity is *v* mm/s. Each frame of image is an average over a range of *Tv* mm along the *X*-direction. In the following, modes 1 and 2 are referred to as the static measurement mode and the continuous measurement mode, respectively.

Figure 10.10 shows the error motions associated with the scanning. As can be seen in Figure 10.10 (a), the error motion along the *Z*-direction does not influence the measurement because the images of the two edges of the slit are taken by the area-image sensor simultaneously. On the other hand, however, the error motion along the *Y*-direction shown in Figure 10.10 (b) directly influences the focus position of the image sensor. Because the depth of focus of a high-magnification objective is only several micrometers, an error motion larger than this amount will introduce errors to the slit width measurement.

Figures 10.11 and 10.12 show the images taken by the image sensor mounted at different *Y*-positions. The image shown in Figure 10.11 was taken at the focus position ($y = 0$ μm) and that shown in Figure 10.12 was taken at a defocus position of 50 μm ($y = -50$ μm) by moving the camera along the *Y*-direction.

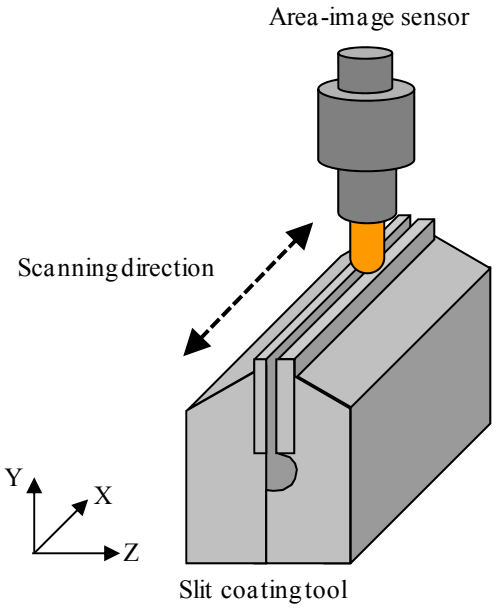

Figure 10.9. Scanning the area-image sensor along the slit

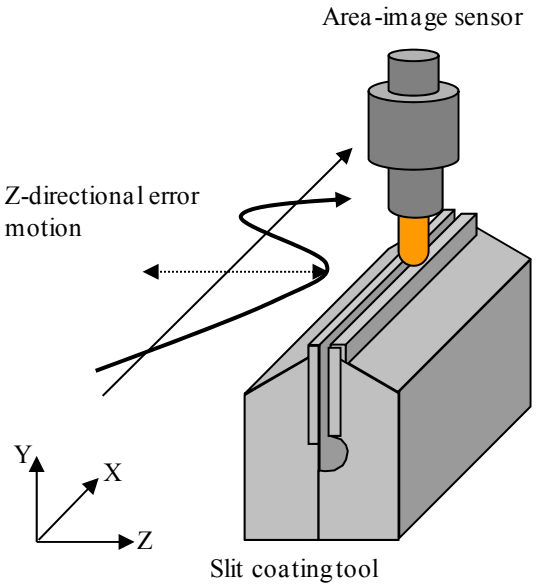

(a) Error motion along the *Z*-direction

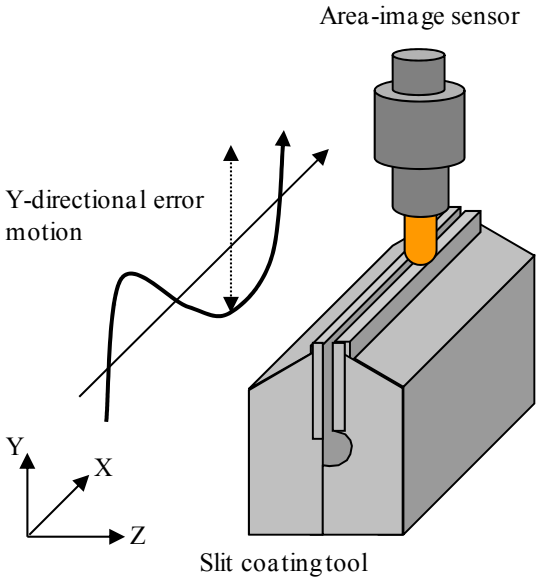

(b) Error motion along the *Y*-direction

Figure 10.10. Scanning error motions

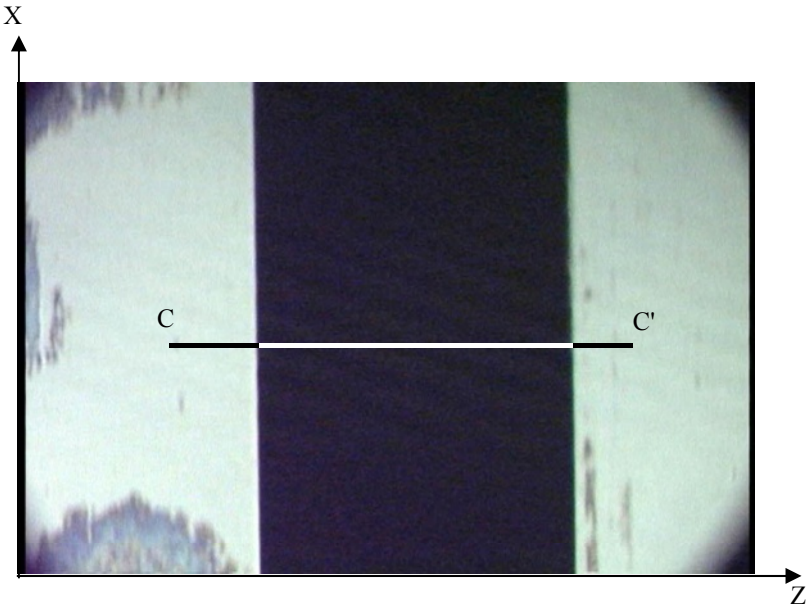

Figure 10.11. An image taken at the focus position (y = 0 μm)

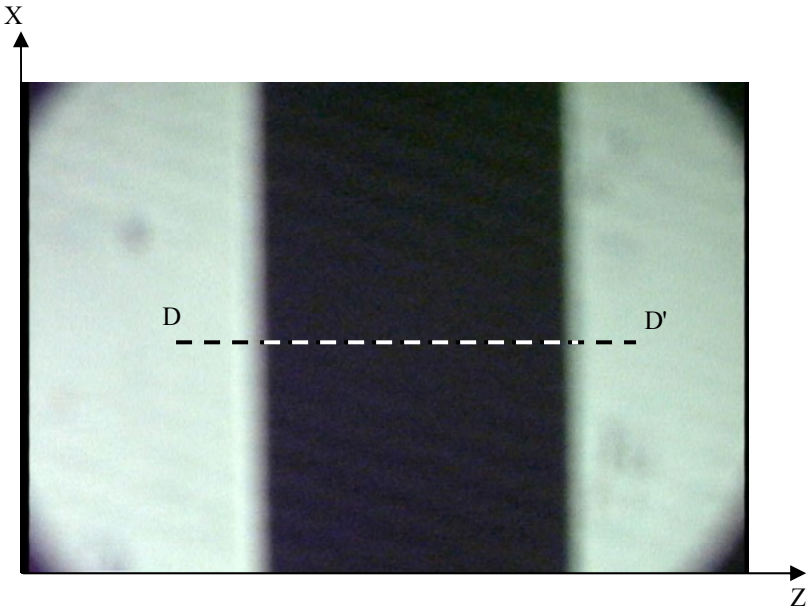

Figure 10.12. An image taken at a defocus position (y = –50 μm)

The influence of the defocus on the image can be observed by comparing the images. The out-of-flatness errors of the top surfaces of the precision elements or tilt of the coating tool also have the same influence. In the static measurement mode, the focus can be re-adjusted at each sampling position to avoid the influence of the *Y*-direction error motion. It is also possible to employ a servo control system for the *Y*-position of the image sensor in the continuous measurement mode. However, this will make the measurement system complicated.

A simple method is proposed to reduce the influence of the *Y*-directional error motion, especially in the continuous measurement mode. In this method, a proper threshold value *T* shown in Equation 10.1 is chosen for the binary processing. Figure 10.13 shows the intensity distributions of the binary images at the line *CC*' in Figure 10.11 and the line *DD*' in Figure 10.12. The binary images were obtained with different threshold values of 127 and 145, respectively. The numbers of pixels of the area-image sensor were 720 and 480 in the *Z*-direction and the *X*-direction, respectively. The corresponding field of view of the image was 310 μm (*Z*) × 230 μm (*X*). As can be seen in the figure, both the left and right edge lines of the intensity distribution of the image taken at $y = -50$ μm shift to the left when compared to that of the image taken at $y = 0$ μm.

The evaluated slit width, which is the distance between the left edge line and the right edge line, changes considerably when the threshold value *T* is set to be 127. On the other hand, the evaluated slit width changes little when *T* is set to be 145. The result indicates that the influence of the *Y*-directional error motion can be reduced by choosing a proper threshold value *T*.

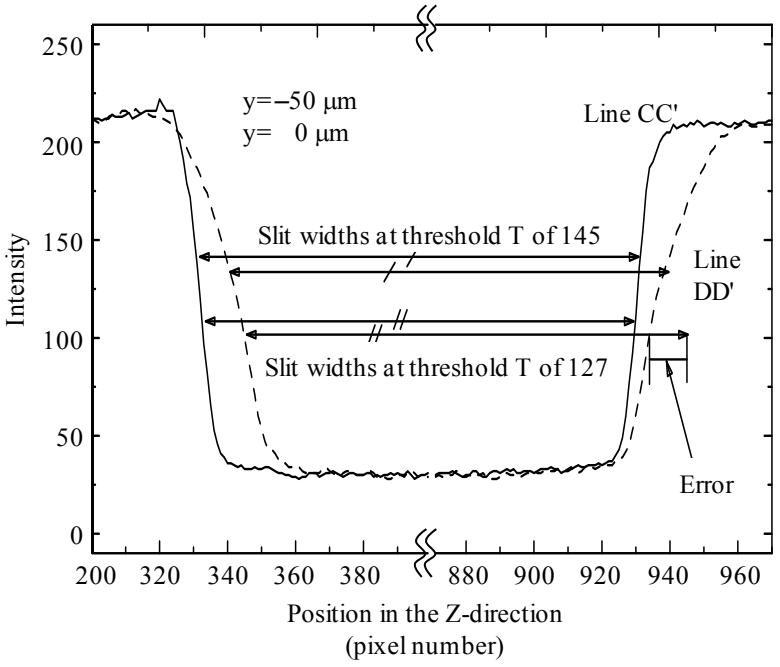

Figure 10.13. Intensity distributions obtained at different *Y*-positions

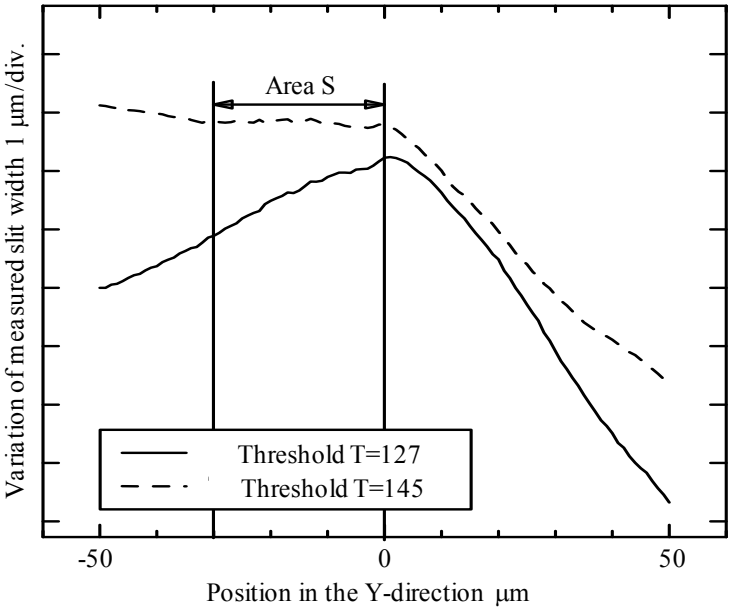

Figure 10.14. Variation of the evaluated slit width with respect to the *Y*-position of the image sensor

Figure 10.14 shows the variation of the evaluated slit width with respect to the *Y*-position of the image sensor. The magnification of the objective lens was set to be 450, corresponding to a field view of 680 μm (*Z*) × 510 μm (*X*). It can be seen that the variation of the evaluated slit width was less than 0.1 μm within the area of *S* (–30 μm < *y* < 0 μm) when the threshold value *T* was set to be 145. It means that the measurement of slit width will not be influenced if the sum of the *Y*-directional error motion and the out-of-flatness of the top surfaces of the coating tool is less than 30 μm.

10.2.4 Slit Width Measurement in Production Line

Slit width measurement of a precision coating tool was also carried out in the production line. Figure 10.15 shows the measurement setup. The precision coating tool was mounted on the worktable of a planer-type surface grinding machine on which the precision elements forming the coating tool had been machined. The area-image sensor with the objective lens was mounted on the grinding head. The image sensor was kept stationary and the coating tool was moved by the worktable along the *X*-direction so that the slit could be scanned by the image sensor.

The width measurement was carried out in the measurement modes of mode 1 (the static measurement mode) and mode 2 (the continuous measurement mode). Table 10.1 shows the measurement parameters.

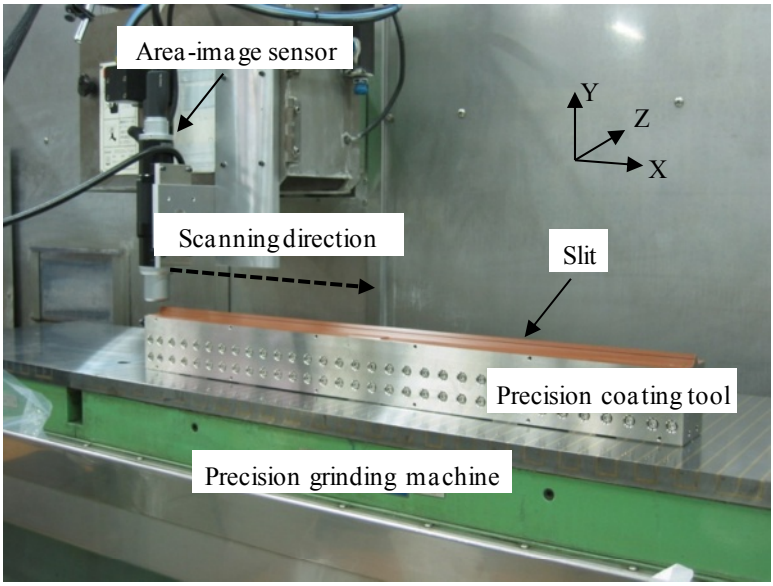

Figure 10.15. Slit width measurement of a precision coating tool on a machine tool

Table 10.1. Measurement parameters

	Mode 1	Mode 2
Length of coating tool	1400 mm	
Nominal width of slit	150 μm	
Numbers of pixels of the area-image sensor	1360 (Z) × 1024 (X)	720 (Z) × 480 (X)
Scanning velocity of the table		42.5 mm/s
Sampling points along the X-direction	14	1000
Measurement time	15 min	30 s

Figure 10.16 shows the measurement results of mode 1 and mode 2. The results of two repeated measurements of mode 1 are shown in Figure 10.16 (a). The results by the conventional thickness gauge are also plotted for comparison. As can be seen in Figure 10.16 (a), the measurement results of mode 1 were consistent with those by the thickness gauge. It can also be seen that the resolution of mode 1 was higher than that of the thickness gauge, which was 0.5 μm for the slit width measurement. Figure 10.16 (b) shows the measurement results of mode 2. The worktable was moved at a velocity of 42.5 mm/s. The measurement time was approximately 30 s, which was much shorter than that of mode 1.

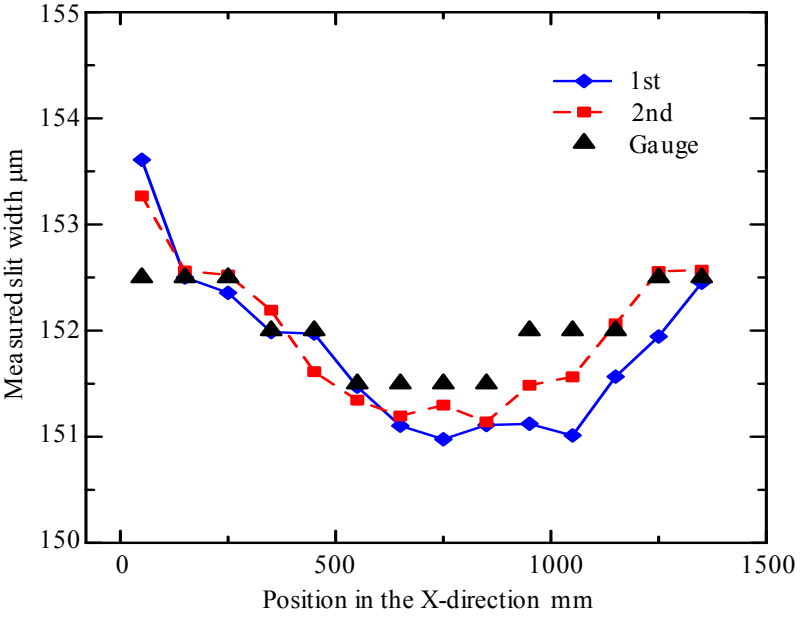

(a) Results by mode 1 and the conventional thickness gauge

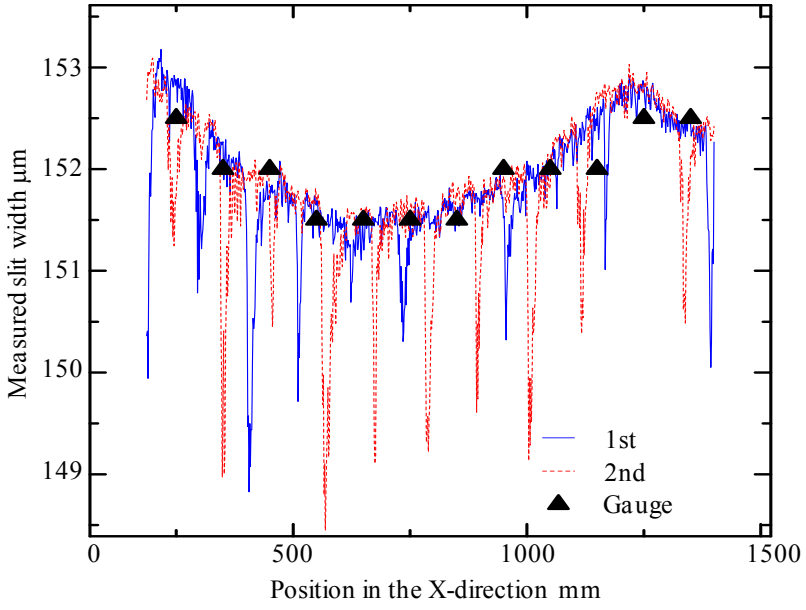

(b) Results by mode 2 and the conventional thickness gauge

Figure 10.16. Results of slit width measurement

The high-frequency components in the results shown in Figure 10.16 (b) were caused by the vibrations from other machine tools operating in the same machine shop. The results were fitted by six-degree polynomial curves to remove the influence of the vibration errors. The fitted results are shown in Figure 10.17. The difference between the two repeated measurement results is also shown in the figure. It can be seen that the repeatability of mode 2 for the slit width measurement was approximately 0.2 μm in Figure 10.17.

Figure 10.18 shows a slit width measuring instrument developed for in-line inspection of precision coating tools based on the technology described in Section 10.2.

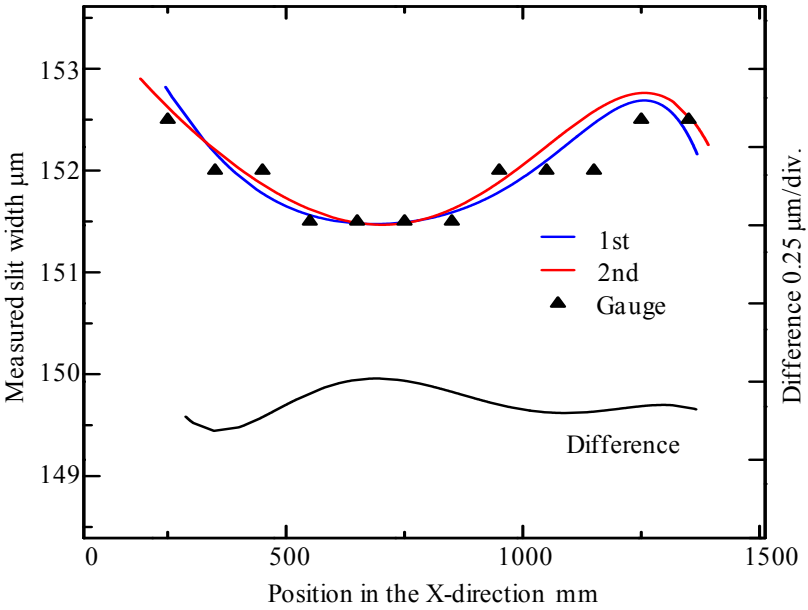

Figure 10.17. Results of slit width measurement by mode 2 after fitting

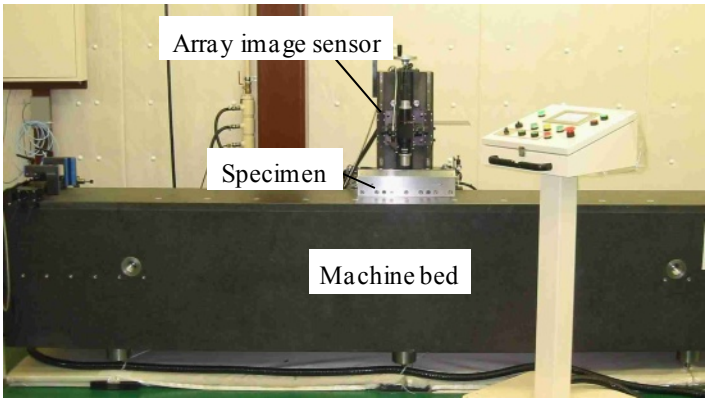

Figure 10.18. A slit width measuring instrument developed for in-line inspection of precision slit coating tools

10.3 Micro-radius Measurement by Scanning Line-image Sensor

10.3.1 Micro-radius of Long Tool Edge

Many tools made by or used in nanomanufacturing have long micro-edges. Figure 10.19 shows an example of this kind of tool. The tool, which is called the extrusion sheet die, is employed in the extrusion of plastic films. Similar to the slot die described in Section 10.2, the extrusion sheet die is configured by combining two precision elements. The length of the tool is up to several meters, and the edge radius of the precision element is less than 100 μm [11]. The function of the extrusion die is to form the desired film shape and dimension. Because the die edges are the final components in the extrusion process, the profiles of the die edges affect most strongly the quality of the extrudate, such as the uniformity, the thickness and the surface roughness. Measurement of the micro-edges, especially the micro-radius, over the entire tool length is thus necessary for quality control of the extrusion process.

Because the size of the tool is too large, it is difficult to mount it on a profile measuring machine for measurement of the edge. Conventionally, the measurement of the edge radius is indirectly measured through replication of the tool edge. Figure 10.20 shows a photograph of taking the replica by using a resin. The shape of the tool edge is transferred to the resin. The replicated edge shape is then measured by using a profile measuring machine. The replication process is time-consuming and the accuracy of replication is also not good enough. Moreover, it is impossible to measure the edge over the entire tool.

In this section, a fast and precision method is described for the measurement of the micro-radius by scanning a line-image sensor.

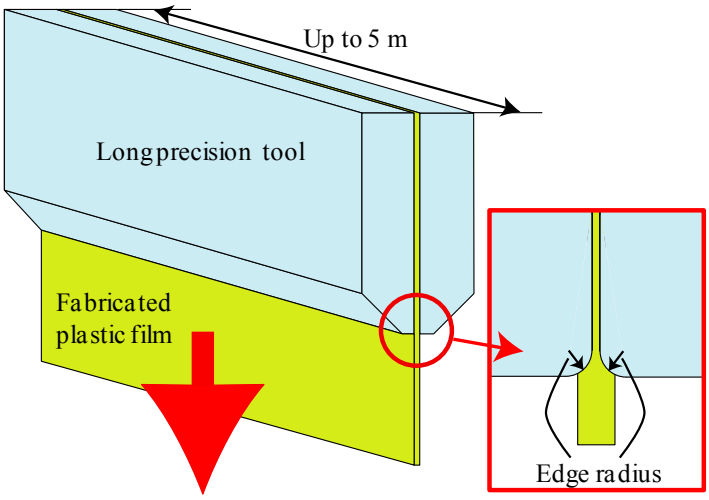

Figure 10.19. A schematic of a long precision tool with micro-edges

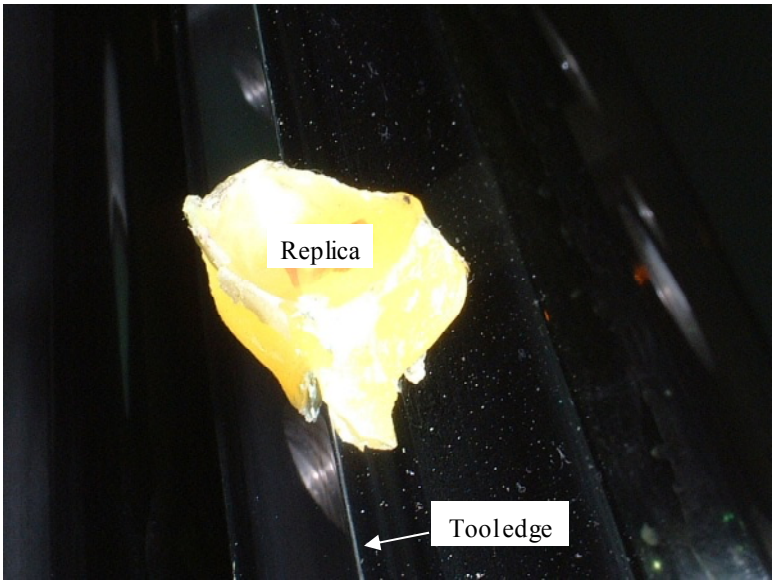

Figure 10.20. Replication of the tool edge in the conventional measurement of the micro-radius

10.3.2 Evaluation of Edge Radius

Figure 10.21 shows a schematic of the measurement system [12]. A line-image sensor with an objective lens [13] is employed to scan the tool edge along the *X*-direction. Figure 10.22 shows a sectional profile of the tool edge in the *YZ*-plane. The edge is assumed to be formed by an arc and two straight lines as shown in the figure. The edge radius is let to be *R*. An illumination light is projected onto the edge along the *Y*-axis. The angle between the incident light and the reflected light is let to be θ. The reflected light intensity is basically a function of the angle θ. The intensity reaches the maximum value when θ is equal to zero and the intensity gets smaller as θ increases. The line-image sensor can only receive the reflected light within a certain range of θ, which is determined by the numerical aperture of the objective lens, the size and sensitivity of the line-image sensor, as well as the reflectivity of the edge surface. Assume the range of the reflected lights, which can be received by the line-image sensor, is from $-\theta_0$ to θ_0. The corresponding edge width can be expressed by:

$$W = 2R\sin\theta_0 . \tag{10.2}$$

Because the edge width *W* can be obtained from the image of the line-image sensor, the edge radius can thus be obtained as:

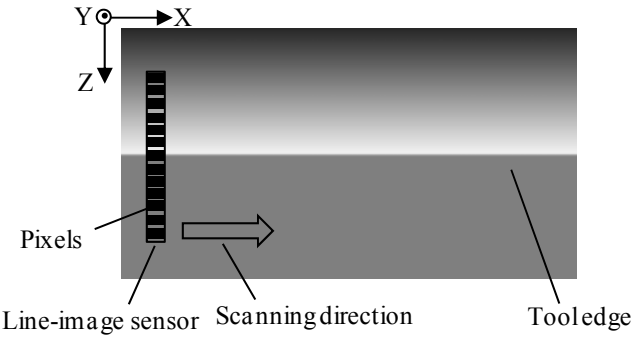

Figure 10.21. Scanning a line-image sensor along the tool edge

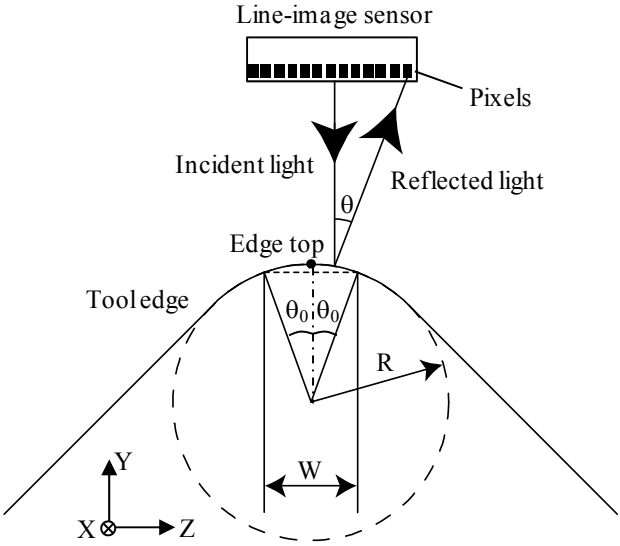

Figure 10.22. Relationship between the edge radius R and the edge width W

$$R = \frac{W}{2\sin\theta_0} = k \cdot W \,, \tag{10.3}$$

where

$$k = \frac{1}{2\sin\theta_0} \,. \tag{10.4}$$

Figure 10.23 shows an image of the tool edge taken by the line-image sensor. Because the line-image sensor can only take one line image along the Z-direction,

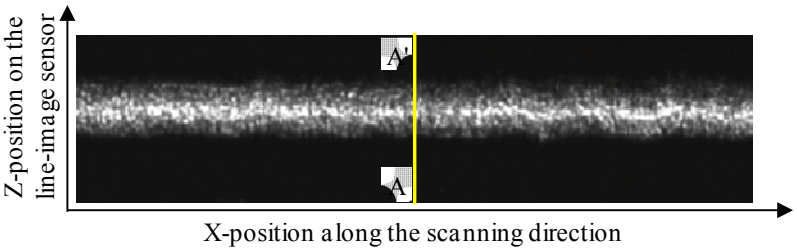

(a) Image of the scanning line-image sensor

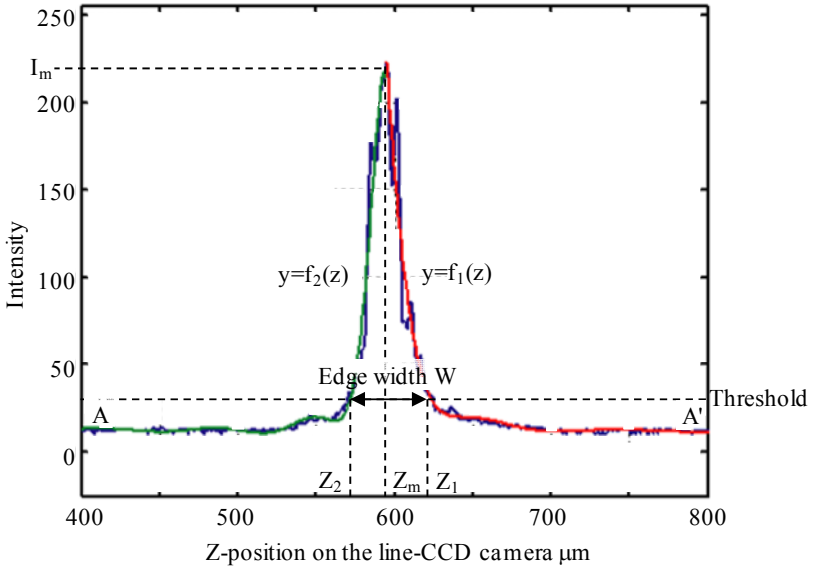

(b) Intensity distribution of line *AA*'

Figure 10.23. An example of the scanned image of the line-image sensor and evaluation of the edge width

it is necessary to scan the sensor along the *X*-direction to get the image of the edge over a certain range of the tool. The intensity output of the sensor at a position of x_i is also shown in the figure. The edge width is evaluated from the sensor output with the following steps:

Step 1: Determine the maximum intensity value I_m and the corresponding pixel position z_m.

Step 2: Fit the intensity curve in the range of $z>z_m$ by a function of $f_1(z)$ and that in the range of $z<z_m$ by a function of $f_2(z)$.

Step 3: Evaluate the pixel positions z_1 and z_2 where $f_1(z_1)$ and $f_2(z_2)$ are equal to a threshold value.

Step 4: Evaluate the edge width as follows:

$$W = z_1 - z_2 \,. \tag{10.5}$$

Because it is difficult to directly calculate the edge radius from the evaluated edge width based on Equation 10.3, a calibration process was introduced to determine the relationship between the edge width and the edge radius by using pin gauges with known radii. The line-image sensor with the objective lens and the lighting unit were mounted on a stepping motor-driven stage with its axis of motion along the *Y*-direction as shown in Figure 10.24. The pin gauge was kept stationary under the sensor. The line-image sensor had 5150 pixels aligned along the *Z*-direction over a length of 36.05 mm. The pixel pitch was 7 μm. The data rate was 40 MHz with a 10-bit video output. The objective lens had a magnification of 10 and a working distance of 50.86 mm. The field of view of the lens was 3.5 mm along the *Z*-direction and the resolution was 0.7 μm. The stepping motor stage has a resolution of 0.02 μm. Table 10.2 shows the specification of the pin gauges used in the calibration. The material of the pin gauge was carbide, which was the same as the tool. Figure 10.25 shows the measured widths of the pin gauges.

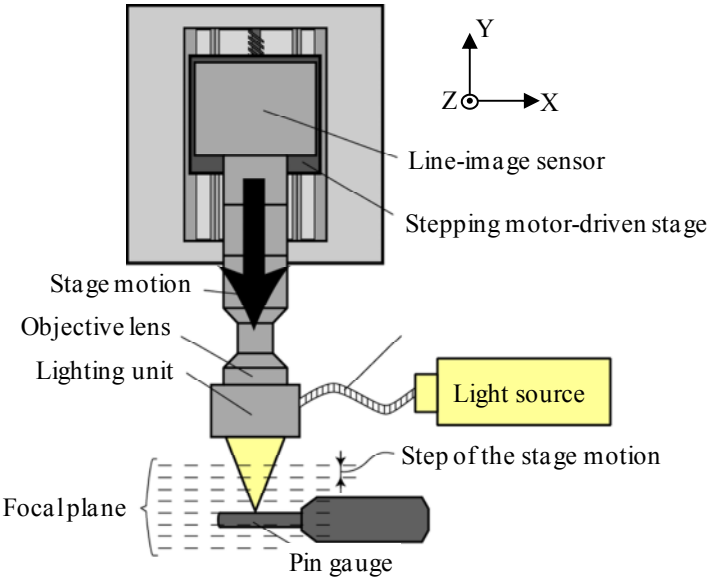

Figure 10.24. Determination of the relationship between the edge radius and edge width

Table 10.2. Specification of pin gauges

Diameter μm	Accuracy μm		Diameter μm	Accuracy μm
50	±0.3		300	±0.1
75	±0.1		400	±0.1
100	±0.1		500	±0.3
150	±0.1		800	±0.3
200	±0.1		1000	±0.4

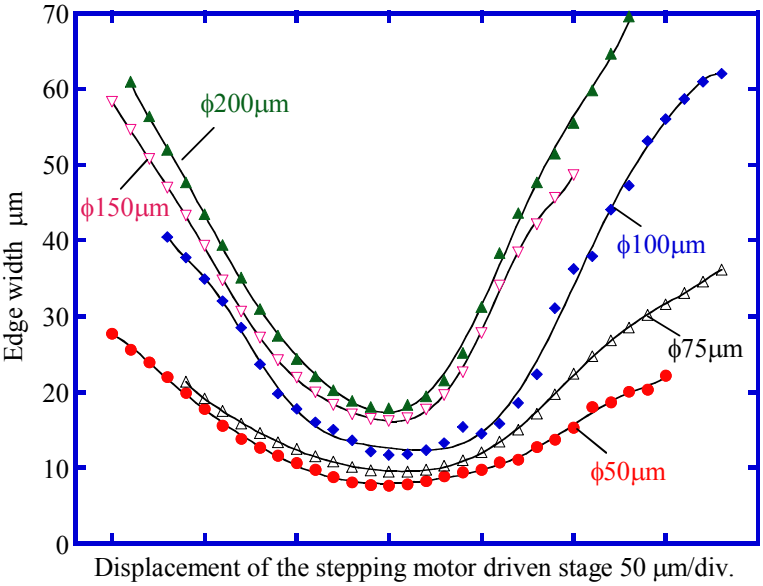

(a) Results of pin gauges with diameters from 50 to 200 μm

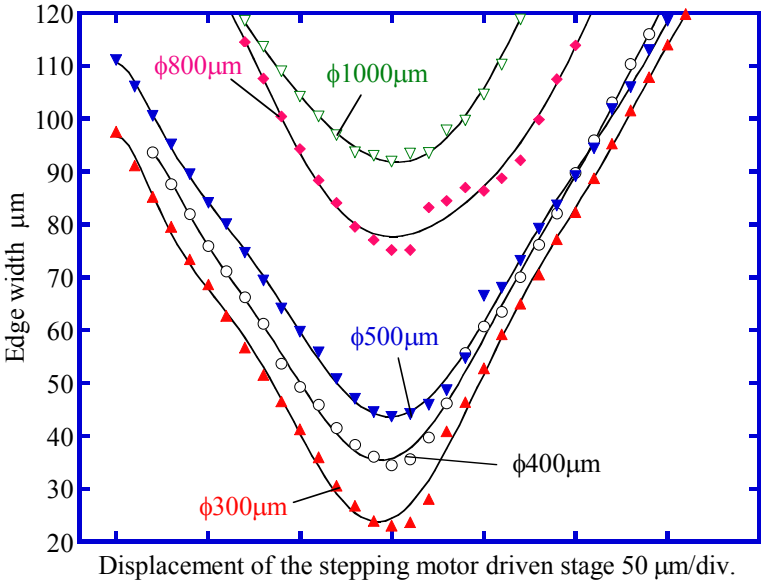

(b) Results of pin gauges with diameters from 300 to 1000 μm

Figure 10.25. Measured widths of pin gauges

In the experiment, the line-image sensor was moved by the stage along the *Y*-direction with a step of 10 μm over a range of 300 μm. At each step, the image of the edge was taken by the sensor to evaluate the edge width. As can be seen in Figure 10.25, the measured edge widths changed with the position of the stepping motor. The minimum was employed as edge width value of the pin gauge, which was obtained at the focus position of the lens. Figure 10.26 shows the relationship between the edge width value and the pin gauge radius. The edge width had a linear relationship with the edge radius. The relationship was employed in the following measurement of the die tool, which is called the width-based method.

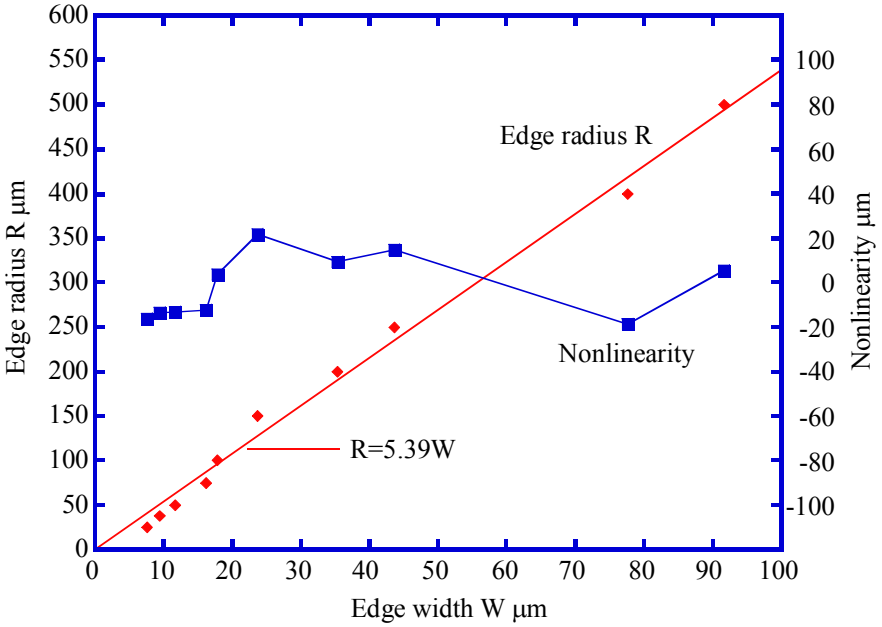

Figure 10.26. Relationship between the edge width and the edge radius

10.3.3 Edge Radius Measurement in Production Line

Figure 10.27 shows a schematic of the measurement system for edge radius of a long extrusion tool in the production line. The tool is kept stationary. The line-image sensor is moved by an *X*-stage to scan the tool edge along the *X*-direction. Because the length of the tool is on the order of several meters, large defocus errors could occur during the scanning, which are caused by the motion error of the scanning stage as well as the tilt and out-of-straightness of the tool edge with respect to the axis of the *X*-stage. As can be seen from Figure 10.25, a defocus error of the image sensor will introduce errors to the edge width measurement. Although it is possible to employ an autofocus mechanism for solving this problem, this will make the measurement longer and the instrument more complicated. As shown in Figure 10.28, multiple *X*-scans are carried out by stepping the image sensor along the *Y*-direction with a *Y*-stage.

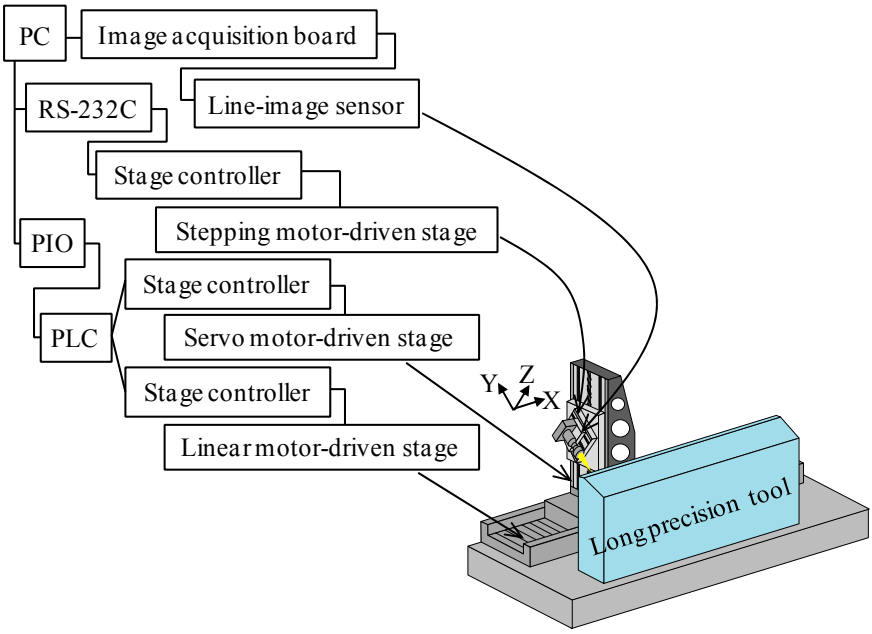

Figure 10.27. Edge radius measurement system for a long extrusion tool

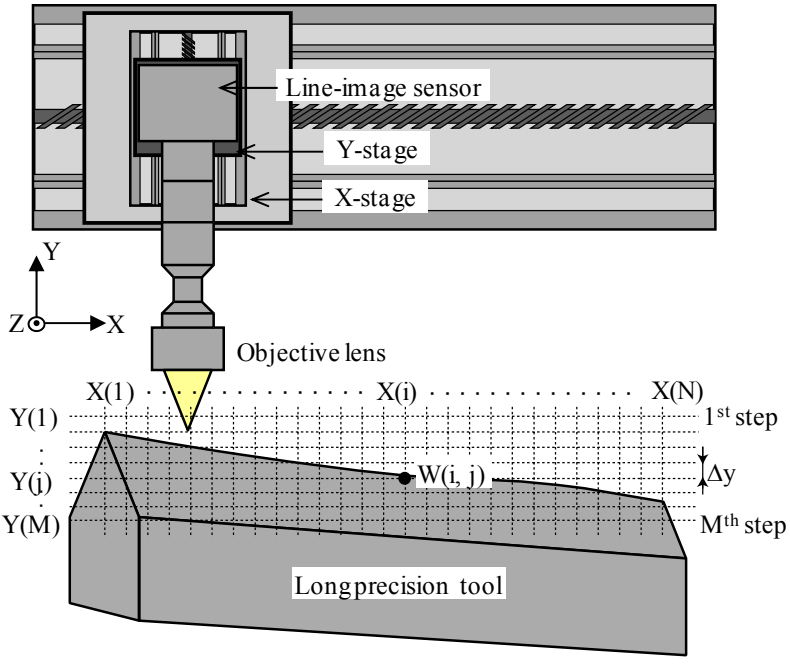

Figure 10.28. Multi-scans for removal of the defocus error

The steps for the scanning of the edge and evaluation of the edge widths are as follows:

Step 1: Set the measurement position along the Y-direction is $Y(1)$. Scan the image sensor along the X-direction to calculate the edge width values $W(i,1)$ ($i = 1, \ldots, N$).

Step 2: Move the Y-stage with a step of Δy so that the measurement position along the Y-direction becomes $Y(2)$. Scan the image sensor along the X-direction to calculate the edge width values $W(i, 2)$ ($i = 1, \ldots, N$).

Step 3: Repeat steps 1 and 2 to get all the edge width values $W(i, j)$ ($i = 1, \ldots, N, j = 1, \ldots, M$).

Step 4: Re-arrange the edge width data to get the curve of $W(i, j)$ with respect to $Y(j)$ ($j = 1, \ldots, M$) at $X(i)$ as shown in Figure 10.29.

Step 5: Determine the edge width at $X(i)$ from the minimum value W_{min} of $W(i, j)$ in Figure 10.29. The corresponding Y_{min} is the focus position at $X(i)$.

Experiments were carried out on a tool with a length of 5 m. The scanning velocity of the X-stage was 100 mm/s. The step Δy in the Y-direction was set to be 10 μm, which was the same as the depth of focus of the objective lens. The number of scans (M) was 14. The total time for taking the images was 30 min. The image shown in Figure 10.30 was called the unit image. There were 5000 lines of the

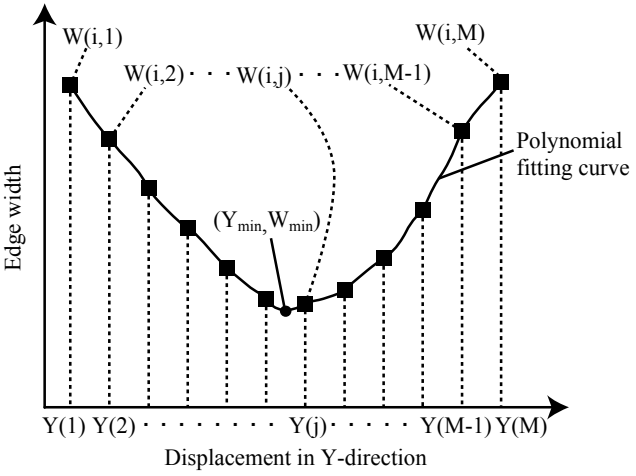

Figure 10.29. Determination of the edge width at $X(i)$

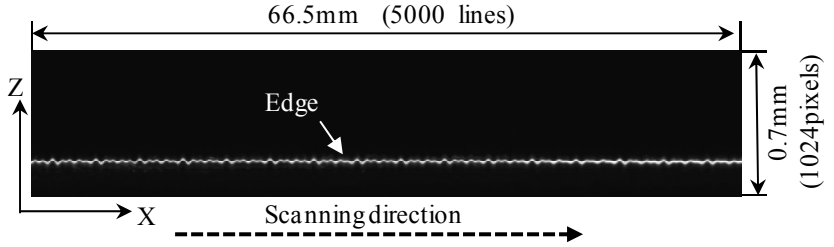

Figure 10.30. Unit image of a part of the tool edge obtained by scanning the line-image sensor ($j = 7$, $X = 2460.5$–2527 mm)

line-image sensor data in the unit image covering a length range of 66.5 mm along the tool edge. Each unit image was stored as an individual data file in the hard disk of the personal computer. There were 78 unit images for the entire tool edge. Figure 10.31 shows the measurement result of the edge radii of the tool. Figure 10.32 shows the corresponding focus position, which was the Y_{min} in Figure 10.29.

The image data obtained in Figure 10.28 can also be employed to evaluate the 3D edge profile by using the method of shape-from-focus (SFF) [14]. As can be seen in Figure 10.33, there are M unit images along the Y-direction. Figure 10.34 shows a schematic of the principle of the SFF method. In this method, the 3D profile of the target surface is measured by taking multiple images at different Y-positions. The Y-directional height position of the surface at the coordinate of (x, z) is determined from the most in-focus image. Figure 10.35 shows the 3D edge profile of the tool by the SFF method, and Figure 10.36 shows the edge radii evaluated from the 3D edge profile data. The results of three repeated measurements are shown in the figure. Comparing the results shown in Figures 10.31 and 10.36, it can be seen that the edge radii evaluated by the two different methods are consistent with each other.

On the other hand, both the width-based method and the SFF method are influenced by the repeatability of the out-of-straightness error motion of the X-directional scanning stage, which was evaluated by using a laser triangular displacement sensor instead of the line-image sensor to scan the side surface of the long tool as shown in Figure 10.37. Figure 10.38 shows a stability of the displacement sensor on the condition of keeping the scanning stage stationary. It can be seen that the sensor output was stable within a range of 0.3 μm. Figure 10.39 (a) shows the sensor output when the sensor was scanning the tool surface. The sensor output $m(x)$ changed approximately 250 μm over the scanning range of 5100 mm, which included the stage out-of-straightness error motion $e(x)$, the out-of-straightness profile error $f(x)$ of the tool surface and the term caused by the tool inclination angle θ. The defocus error caused by $m(x)$ to the image sensor can be removed by the method shown in Figures 10.28 and 10.33 on the condition that the repeatability of $m(x)$ is less than the depth of focus of the objective lens. The scanning was repeated sixteen times to investigate the repeatability of $m(x)$. The results are shown in Figure 10.39 (b). The repeatability of $m(x)$, which was mainly the repeatability of the stage motion, was approximately 1.5 μm. It can be seen that the repeatability, which was much smaller than the 10 μm depth of focus of the objective lens, was good enough for the measurement of the edge radius.

Figure 10.40 shows a photograph of an edge radius measuring instrument developed for in-line inspection of long extrusion tools based on the technology described in Section 10.3.

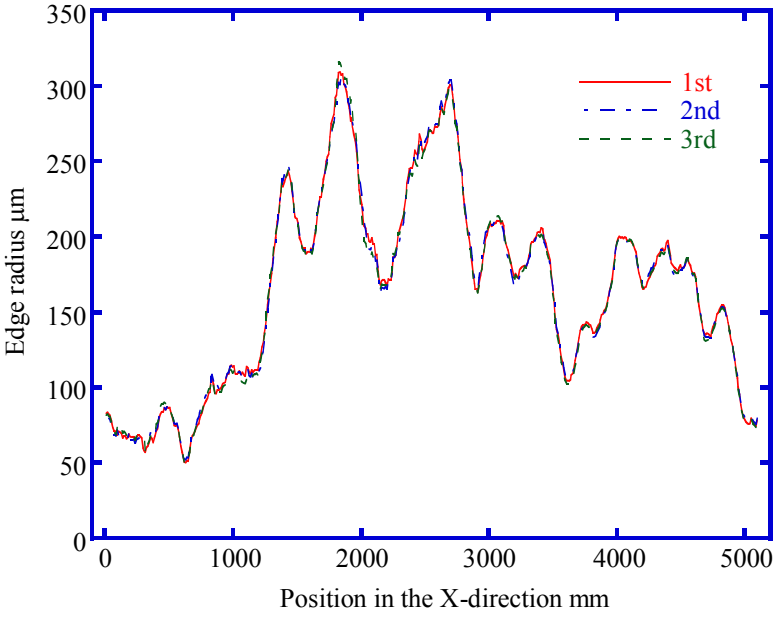

Figure 10.31. Results of three repeated measurements of the edge radii of the long tool by the width-based method

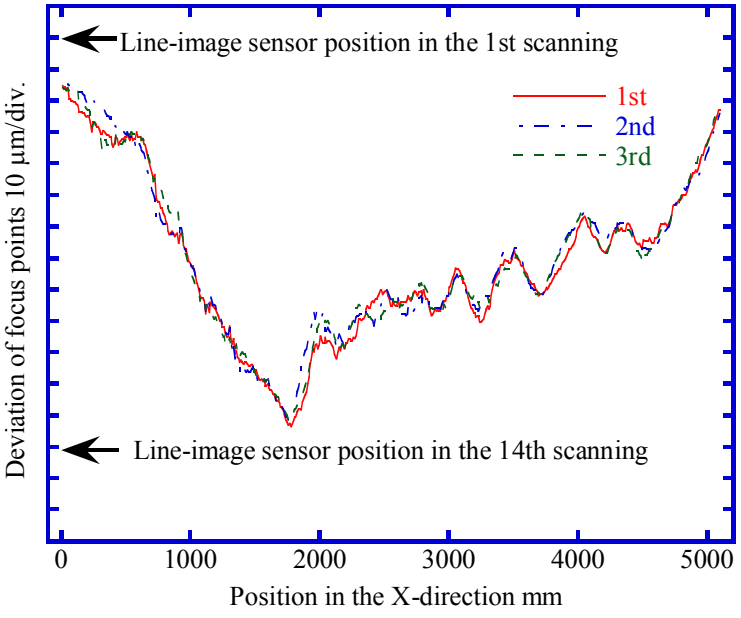

Figure 10.32. Results of three repeated measurements of the focus points of the line-image sensor in the *Y*-direction

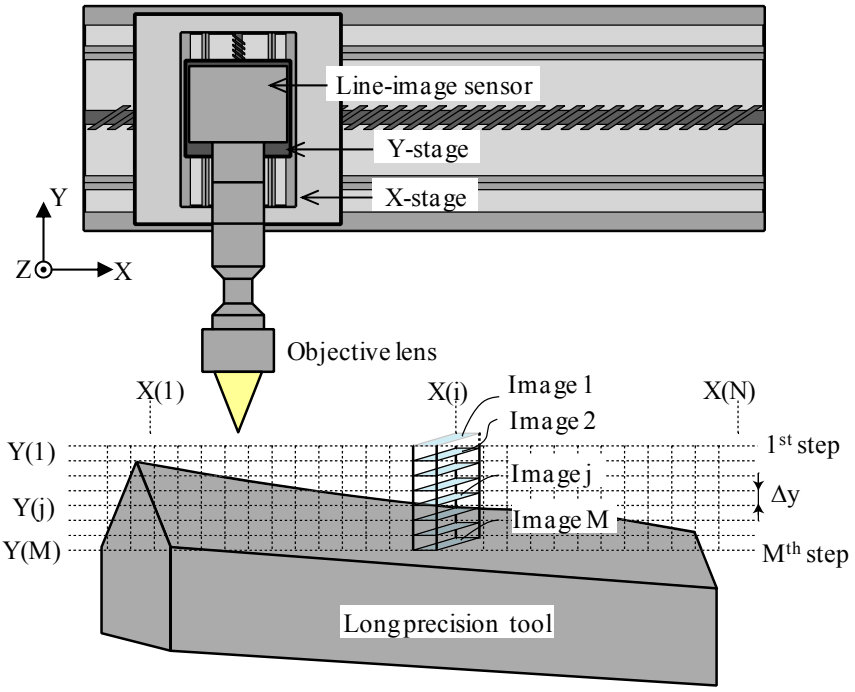

Figure 10.33. Results of three repeated measurements of the edge radii of the long tool

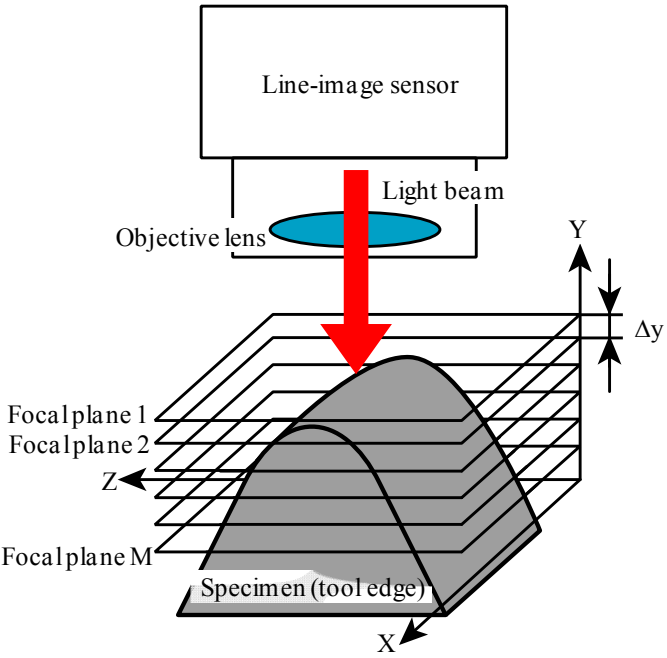

Figure 10.34. Principle of the SFF method

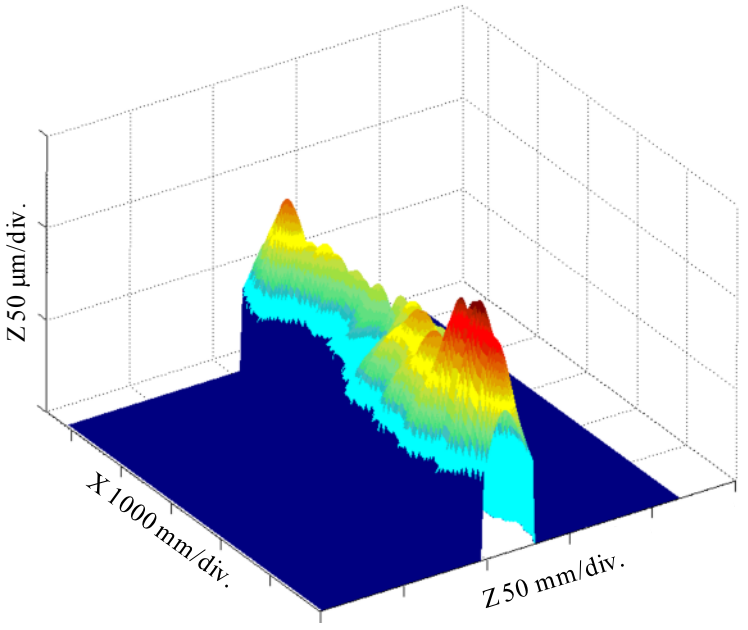

Figure 10.35. 3D edge profile of the long tool by the SFF method

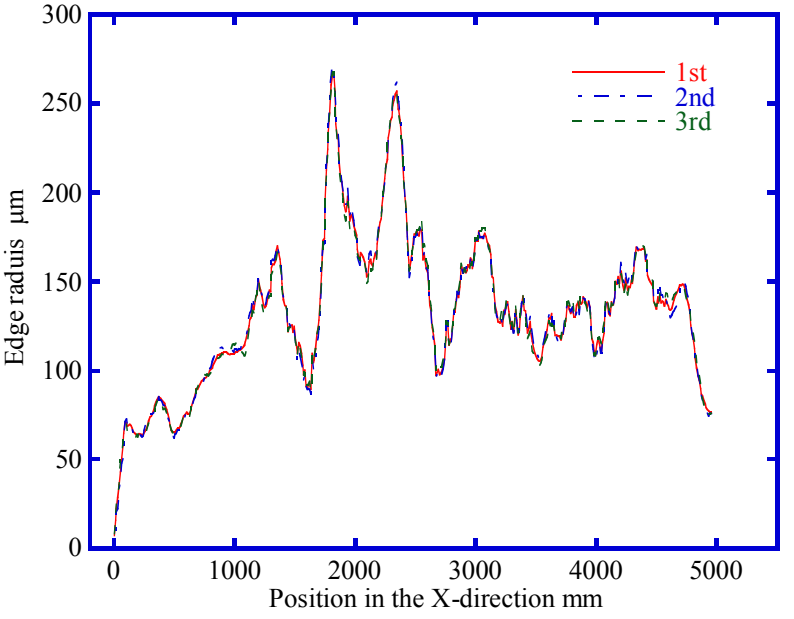

Figure 10.36. Results of the edge radii of the long tool by the SFF method

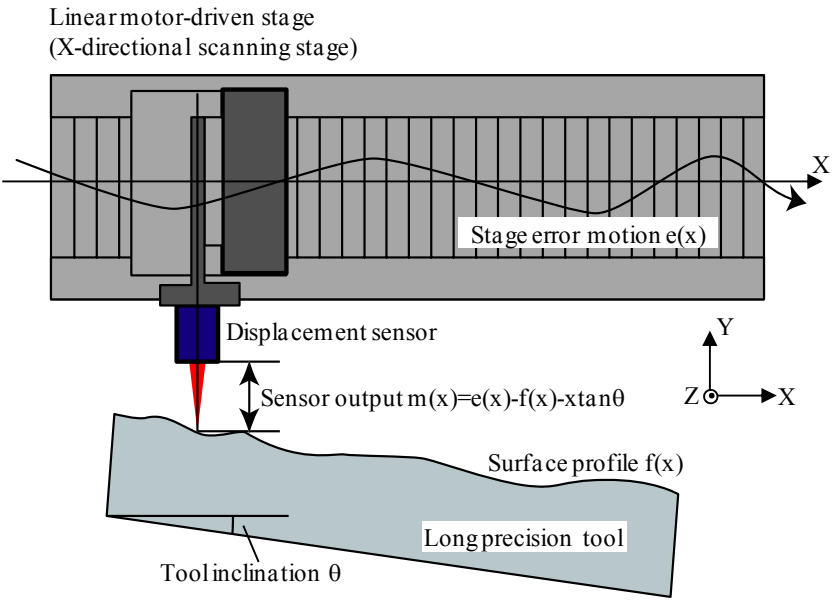

Figure 10.37. Setup for investigating the repeatability of the out-of-straightness error motion of the *X*-directional scanning stage

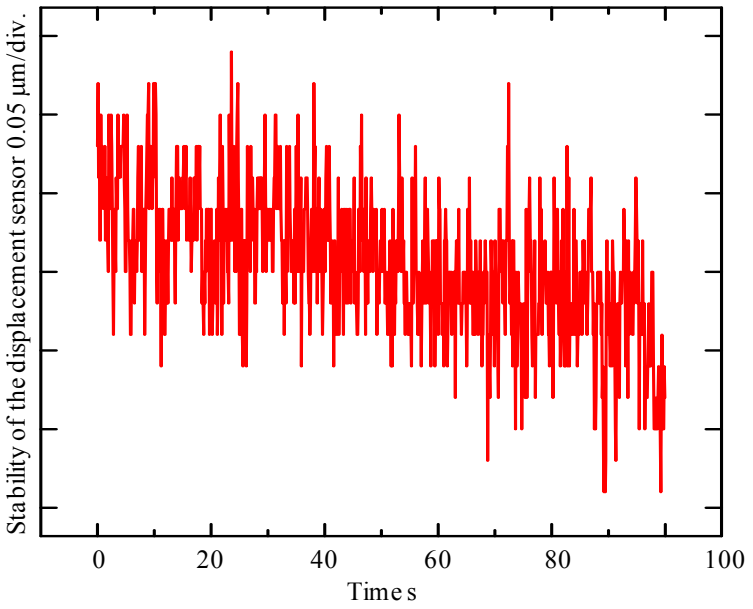

Figure 10.38. Stability of the displacement sensor for scanning

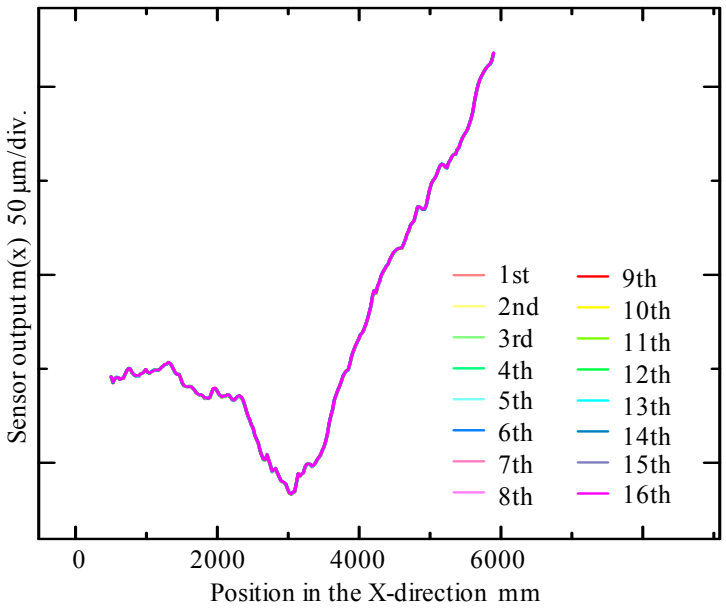

(a) Output of the displacement sensor

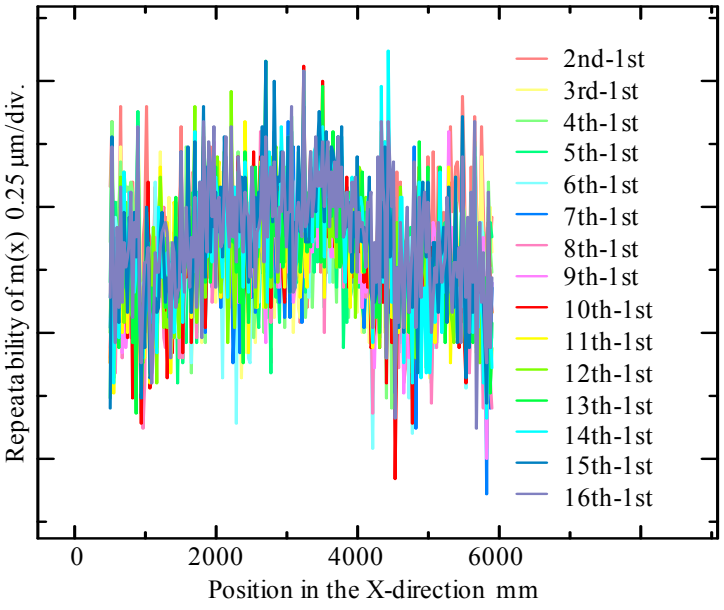

(b) Repeatability of the out-of-straightness error motion

Figure 10.39. Investigation of the repeatability of the out-of-straightness error motion of the *X*-directional scanning stage

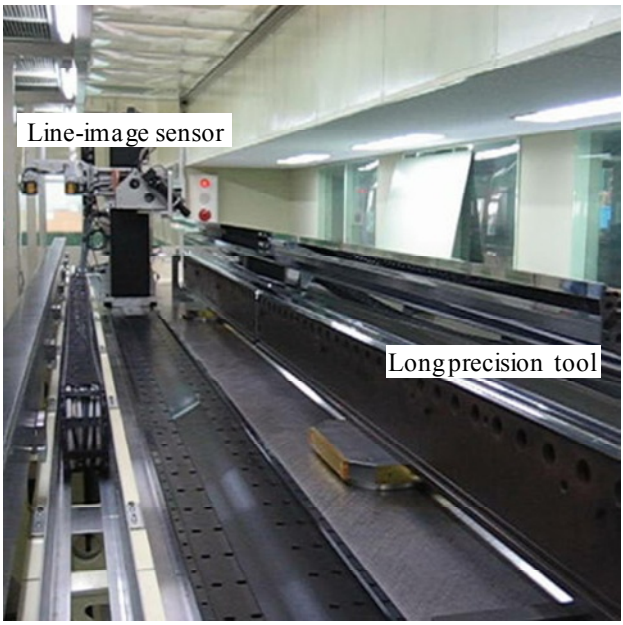

Figure 10.40. An edge measuring instrument developed for in-line inspection of long extrusion tools

10.4 Summary

Scanning image-sensor systems are effective for fast measurement of micro-dimensions over long ranges. Two systems have been presented for measurement of micro-dimensions of precision long tools.

The first is a scanning area-image-sensor system employed for measurement of micro slit width of a long coating tool. The image of the two slit edges is captured by an area-image sensor. The image is processed using binarization to detect quickly the edge positions of the slit. The slit width is determined through a least square linear fitting of the edge data from binary image. The influence of the *Z*-directional straightness of the scanning stage can be reduced by choosing a proper threshold for binarization of the image. The slit width over the entire length of a 1.4 m long coating tool was measured in 33 s.

The second system is for a micro-edge radius measurement of a long extrusion tool by scanning a line-image sensor. In the width-based method, the edge width of the tool at each scanning point is first evaluated from the image of the line-image sensor. The edge radius is then calculated from the edge width based on the calibration results using pin gauges. A multi-line scanning method has been employed to reduce the influence of the defocus error caused by the out-of-straightness error motion of the scanning stage. The multi-line scanned images have also been applied to the shape-from-focus (SFF) method. This method uses

different focus levels to obtain a sequence of the images of the target surface in the same field of view of the image sensor. The edge radii of a 5100 mm long precision tool was measured within a measurement time of 30 min. Consistent results of edge radii have been obtained by the width-based method and the SFF method.

References

[1] Barrett RC, Quate CF (1991) Optical scan-correction system applied to atomic force microscopy. Rev Sci Instrum 62(6):1393–1399
[2] Asada N, Fujiwara H, Matsuyama T (1998) Edge and depth from focus. Int J Comput Vis 26(2):153–163
[3] Wang CC (1994) A low-cost calibration method for automated optical measurement using a video camera. Mach Vis Appl 7:259–266
[4] Baba M, Ohtani K (2001) A novel subpixel edge detection system for dimension measurement and object localization using an analogue-based approach. J Opt A Pure Appl Opt 3:276–283
[5] Fan KC, Lee MZ, Mou JI (2002) On-line non-contact system for grinding wheel wear measurement. Int J Adv Manuf Technol 19:14–22
[6] Ferron Magnetic Inks (2010) http://www.ferron-magnetic.co.uk/coatings/index.html. Accessed 1 Jan 2010
[7] Ryotec (2009) http://www.ryotec.co.jp/english/index.html. Accessed 1 Jan 2010
[8] Furukawa M, Gao W, Shimizu H, Kiyono S, Yasutake M, Takahashi K (2003) Slit width measurement of a long precision slot die. J JSPE 69(7):1013–1017 (in Japanese)
[9] Keyence Corporation (2010) CCD camera, http://www.keyence.com. Accessed 1 Jan 2010
[10] Gonzalez RC, Woods RE (2002) Digital image processing. Prentice Hall, Upper Saddle River, NJ
[11] Kostic MM, Reifschneider LG (2006) Encyclopedia of chemical processing. Taylor and Francis, London
[12] Motoki T, Gao W, Furukawa M, Kiyono S (2007) Development of a high-speed and high-accuracy measurement system for micro edge radius of long precision tool. J JSPE 73(7):823–827 (in Japanese)
[13] Nippon Electro-Sensory Devices Corporation (2010) http://www.ned-sensor.co.jp. Accessed 1 Jan 2010
[14] Nayer SK, Nakagawa Y (1994) Shape from focus. IEEE Trans PAMI 16(8):824–831